IEEE Access
Multidisciplinary | Rapid Review | Open Access Journal

Received 3 January 2023, accepted 18 January 2023, date of publication 23 January 2023, date of current version 30 January 2023.

Digital Object Identifier 10.1109/ACCESS.2023.3239209

RESEARCH ARTICLE

A Load-Independent Fission-Type Inductive Power Transfer System for 3D Reconfigurable IoT Array

YIMING GAO[1,2,3], ZIJIE CHEN[1,4], HAOYU WANG[1,4], (Senior Member, IEEE), YU LIU[1,4], (Senior Member, IEEE), MINFAN FU[1,4], (Senior Member, IEEE), AND JUNRUI LIANG[1,4], (Senior Member, IEEE)

[1]School of Information Science and Technology, ShanghaiTech University, Shanghai 201210, China
[2]Shanghai Advanced Research Institute, Chinese Academy of Sciences, Shanghai 201210, China
[3]University of Chinese Academy of Sciences, Beijing 100049, China
[4]Shanghai Engineering Research Center of Energy Efficient and Custom AI IC, Shanghai 201210, China

Corresponding author: Junrui Liang (liangjr@shanghaitech.edu.cn)

This work was supported in part by the National Natural Science Foundation of China under Grant 62271319 and Grant U21B2002, and in part by the Natural Science Foundation of Shanghai under Grant 21ZR1442300.

ABSTRACT In recent years, the number of electronic devices and appliances that support wireless charging has rapidly increased, owing to the research and development breakthroughs in inductive power transfer (IPT) technology. The existing wireless charging protocols, such as Qi and AirFuel, support only a few devices to be charged simultaneously. They cannot be directly utilized to construct a complex IPT network. This article introduces a reconfigurable three-dimensional (3D) IPT system based on series-parallel (SP) compensation for wirelessly powering multiple adjacent cubic Internet of Things (IoT) devices. These cubes can be configured into different 3D array combinations according to the application demands. After the 3D cube array is formed, a self-detection mechanism runs to turn off the uncoupled coils, such that to maximize the power transmission efficiency of the entire system. These cubes serve as not only IoT loads but also wireless power relays. In this way, the number of loads is not limited by the size of a single transmission coil. In addition, it maintains a constant drive voltage to each load device, regardless of the load variations in local or adjacent cubes. The constant voltage design eases local power management. A prototyped IPT cube array is manufactured and tested to validate the proposed idea. This fission-type IPT system makes a valuable exploration of the 3D IPT technology toward future ubiquitous and reconfigurable IoT arrays.

INDEX TERMS Inductive power transfer, Internet of Things, load-independent system, reconfigurable 3D array, wireless power relay.

I. INTRODUCTION

Indctive power transfer (IPT) technology cuts the last cord between the power supply and electrical appliances. It offers many advantages such as safety, flexibility, and cleanliness. Thanks to these advanced features, IPT has become a promising power solution in some cutting-edge applications, such as implantable medical devices [1], intelligent home applications [2], [3], and electric vehicle [4]. Owing to the breakthroughs in IPT technology over the last decade, the number of devices that support wireless charging grows rapidly. However, most existing IPT systems only support one-to-one (single transmitter and single receiver) structure [5], as shown in Fig. 1(a). The specific connections limit the number of devices that can be charged simultaneously. The AirFuel Alliance wireless power transfer (WPT) system [6] can provide up to eight power receiver units (PRUs), as shown in Fig. 1(b). Nevertheless, it is still not comparable to the growing number of PRUs, especially for those in spatial distributed Internet of Things (IoT) applications.

The associate editor coordinating the review of this manuscript and approving it for publication was Alon Kuperman.

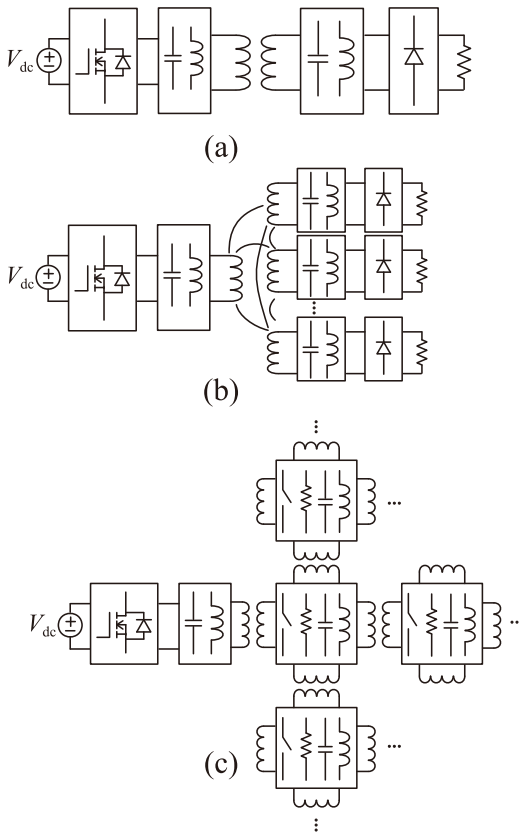

FIGURE 1. IPT structures. (a) One-to-one IPT. (b) One-to-N IPT. (c) Proposed fission-type IPT.

On the other hand, although there are some ambient energy harvesting technologies that can be utilized to power spaciously distributed IoT devices [7], [8]. The available power level is much lower than that the active IPT can provide. Therefore, it is necessary to develop three-dimensional (3D) IPT technology to meet the demand for flexibly configurable and more power-hungry IoT applications.

To satisfy the wireless charging demand of more load devices, the IPT systems supporting multiple PRUs have been studied in some literature [9], [10], [11], [12], [13]. By using the multi-load IPT system, the number of power inverters can be reduced; the power density increases [14]. In [9], an IPT system with two layers of primary coils is implemented for desktop peripherals, such as a mouse, keyboard, and loudspeaker at every position on the table. Other multiple PRUs IPT technologies were also observed from time to time, for example, the omnidirectional WPT charging bowl proposed in [10]. Multiple PRUs can be placed at any position in the bowl to be charged simultaneously without strict positional confinement. In [11], the concept of three roles in a multi-node IPT system is proposed to balance the transferred power, transfer distance, and dynamic power variation requirements by changing the roles of different nodes.

As pointed out in [15], the cross-coupling among the multiple PRUs cannot be disappeared, leading to interference among different loads. On the other hand, from the load point of view, a constant voltage (CV) is preferred. Nevertheless, without a specific design, either the local or the neighbors' load variations might affect the local output voltage. To maintain the CV characteristic for the load, a dc/dc converter is used as a voltage regulator in [16] and [17]. In [18], multiple double-T resonant circuits are connected for multiple PRUs, such that to maintain CV outputs. Sun et al. [19] studied the frequency conditions of the multiple PRUs and realized the CV characteristics by making a series compensation to each coil.

Besides the number of receivers, the transfer distance and charging area are also of concern. These performances can be further increased and extended by introducing wireless power relays. In [16], a reconfigurable two-dimensional (2D) wireless charging system is implemented to extend the charging area using multi-hop and dynamic power routing. In [20], [21], [22], [23], [24], and [25], some domino-type inductive power relay systems are reported. In these designs, each relay consists of two coils, one for receiving the wireless energy from the upstream device and the other for transmitting it to the downstream device, respectively. They used appropriate circuit topologies and well-designed magnetic coil couplers to realize the CV characteristic in the series-relaying multi-load IPT systems.

In this paper, we proposed a novel fission-type IPT system based on series-parallel (SP) compensation as Fig. 1(c) shows. Every battery-free cubic cell in this system serves as a power relay with local CV output. The smart IPT cubes are reconfigurable to form any 3D array according to the application demand. They can detect the availability of the adjacent cells and disconnect the uncoupled coils, such that to enhance the energy transmission efficiency. The feasibility and performance of the proposed system have been evaluated in several experiments. The proposed fission-type IPT system has extended the wireless charging range of the neighboring IoT devices. The purpose is to explore the future wide-range IPT technology for ubiquitous IoT systems.

The rest of this paper is organized as follows. The system structure is introduced in Section II. The transfer capabilities analysis is presented in Section III. The feasibility and performance of the proposed system are evaluated in several experiments in In Section IV. Section V concludes this article.

II. SYSTEM CONFIGURATION

The proposed fission-type IPT system is formed by many cubic IoT units. Each cube is an independent IoT node. Various sensors, digital microprocessors, screens, and network interfaces are embedded inside each cube to make it intelligent. When a cube is connected to a neighboring unit, it receives power from the neighboring unit for local usage and also relays the electricity to its neighbors. Fig. 2 shows the conceptual IoT array with reconfigurable displays, which are powered by the proposed IPT technology. Before configuration, all cubes are off work and randomly placed as shown in Fig. 2(a). In order to satisfy different display demands, the IoT cubes can be configured in either

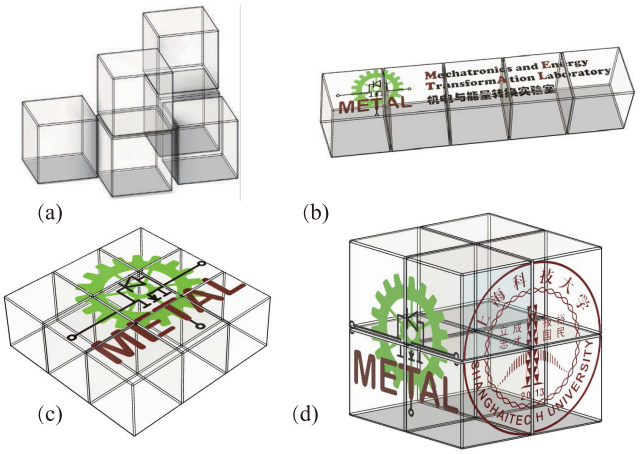

FIGURE 2. IPT system for conceptual reconfigurable IoT display array. (a) Before configuration. (b) One-dimensional configuration. (c) Two-dimensional configuration. (d) Three-dimensional configuration.

one-dimensional (1D), 2D, or 3D arrays, as shown in Fig. 2(b)–(d). On each face of a cube, there is a printed circuit board (PCB) coil for power exchange from/to the neighboring cube. Such a 3D cubic design enables the wireless power relay in any spatial direction, which significantly extends the range and convenience of electric power delivery in the 3D space.

A. CUBE UNIT

In the fission-type reconfigurable IPT cube system, all cubic cells have an identical circuit topology, as shown in Fig. 3(a). To analyze the system, some basic definitions are given as follows. Each cube consists of six circuit branches, which represent the coils on the six faces of a cube and their corresponding compensating components. The six branches are connected in parallel with an equivalent ac load R_{ac}. Owing to the PCB manufacturing consistency, the coil inductance and equivalent series resistance (ESR) of each coil are almost identical; therefore, they are denoted as the same notions for simplicity. Each branch consists of a coil inductor L, a series compensating capacitor C_1, and a parallel compensating capacitor C_2. Each coil has an ESR r. The operation frequency of the power source is f. The corresponding angular frequency is $\omega = 2\pi f$. The mutual inductance between two adjacent cubes is denoted as M. The parameter M can also be regarded as a constant value because the relative position between two cubes is fixed by using some additional permanent magnetic locks. Therefore, the coupling coefficient $k = M/L$ between adjacent cubes is also a constant number. The quality factor of a coil is defined as follows

$$Q = \frac{\omega L}{r}. \tag{1}$$

Six electronic switches S_1–S_6 control whether or not the corresponding branches are connected to the system. If there is an adjacent cube detected, the system turns on the corresponding branch for bidirectional wireless power transfer; if not, it disconnects the very branch.

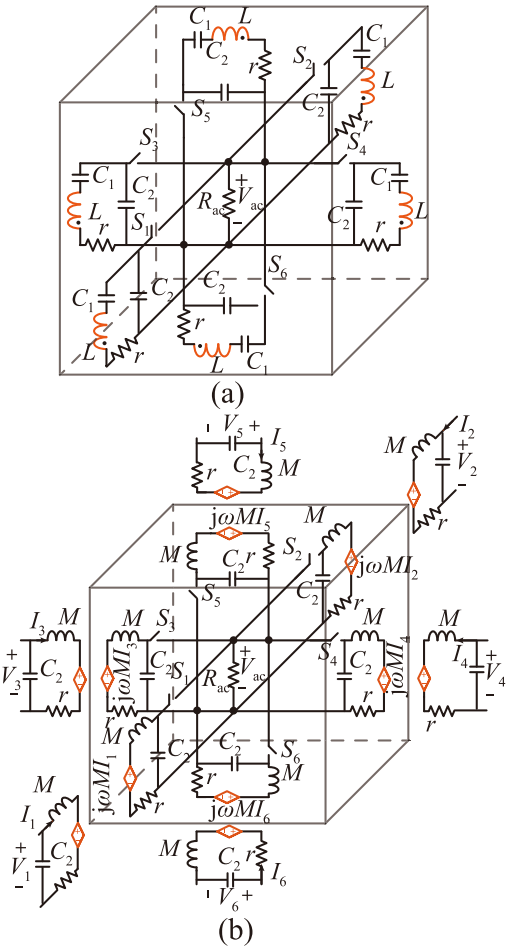

FIGURE 3. Circuit topology of one cube in the proposed IPT system. (a) Circuit topology. (b) Equivalent circuit.

In the proposed circuit topology, the values of the compensating capacitors C_1 and C_2 are designed as follows

$$C_1 = \frac{1}{\omega^2(L-M)}, \tag{2}$$

$$C_2 = \frac{1}{2\omega^2 M}, \tag{3}$$

such that the equivalent impedance of each cube exhibits a resistive value and the load voltage magnitude can maintain constant.

B. CONSTANT VOLTAGE OUTPUTS

The equivalent circuit model of a cubic unit is shown in Fig. 3(b). According to (2), the capacitive reactance C_1 balances some of the inductive reactance of the coil inductance L, making the remaining inductance equal to M. For a general case, suppose that there exist six identical cubes adjacent to the six faces of the studied cube, as illustrated in Fig. 3(b). The phasors of branch currents of the six adjacent cubes are denoted as I_1 to I_6, respectively. The phasors of load

ac voltages of the adjacent cubes are denoted as V_1 to V_6, respectively. In the proposed fission-type IPT system, a face of a cube must be aligned and abut against one of the six faces of another cube, in order to exchange power between the two cubes. The cross-coupling between the non-abutting coils is weak; therefore, it is neglected in the circuit model analysis. Based on the nodal analysis, the governing equation of a studied cube is formulated as follows

$$\left(\frac{jkQ+1}{k^2Q^2}+\frac{jkQ+1}{jkQ}\frac{r}{R_{ac}}+\frac{jkQN}{jkQ+1}\right)V_{ac}=\sum_{n=1}^{N}V_n, \quad (4)$$

where N is the number of effective adjacent cubes. The quality factor Q is a constant much larger than one. Its typical value is often greater than 100 when the operation frequency is 6.78 MHz. The coupling coefficient k is less than one. With these prerequisites, (4) can be simplified into

$$\left(\frac{r}{R_{ac}}+N\right)V_{ac}=\sum_{n=1}^{N}V_n. \quad (5)$$

Further, when the load resistance R_{ac} is much larger than the ESR r, the ac voltage across the equivalent ac resistor can be further simplified into the following equation

$$V_{ac}=\frac{1}{N}\sum_{n=1}^{N}V_n. \quad (6)$$

From (6), V_{ac} the voltage phasor across R_{ac} is the average of those ac voltages in its adjacent cubes. V_{ac} is independent of the equivalent ac load under the ideal conditions. Given that V_{ac} describes the voltage of an arbitrary cube in the 3D-IPT network, a stable solution is attained when all the cell voltages are equal. Therefore, the CV feature is realized against the load variations and fluctuations in the distributed cubes.

C. ZERO-PHASE-ANGLE (ZPA) ANALYSIS

When the reactive parts in a unit cube is balanced, it exhibits a pure resistive impedance to its adjacent cube. A ZPA is achieved between the branch voltage and current. When all cubes exhibit a resistive outlook, the drive inverter gives the minimum switching loss. Therefore, the ZPA analysis is of important to optimize the power transmission efficiency. In this proposed design, ZPA can be realized by turning off all the uncoupled branches of a cube.

Fig. 4(a) shows how the switches work to realize the ZPA characteristics. When two cubes are connected, their coupled branches should be switched on, While other uncoupled branches are turned off. Given that the uncoupled branches are disconnected or open-circuited, the simplified circuit is shown in Fig. 4(b). In the corresponding T-model, which is shown in Fig. 4(c), if the ESR r is small enough to be neglected and the resonant conditions (2) and (3) are satisfied, the branch input impedance is just

$$Z_{in}=R_{ac}. \quad (7)$$

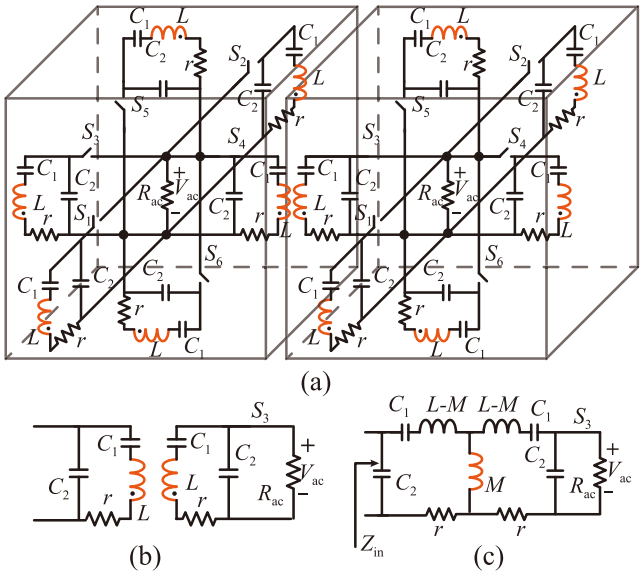

FIGURE 4. Two coupled cubes for zero-phase-angle analysis. (a) Equivalent circuit. (b) Simplified coupling branches. (c) T-model of the simplified branches.

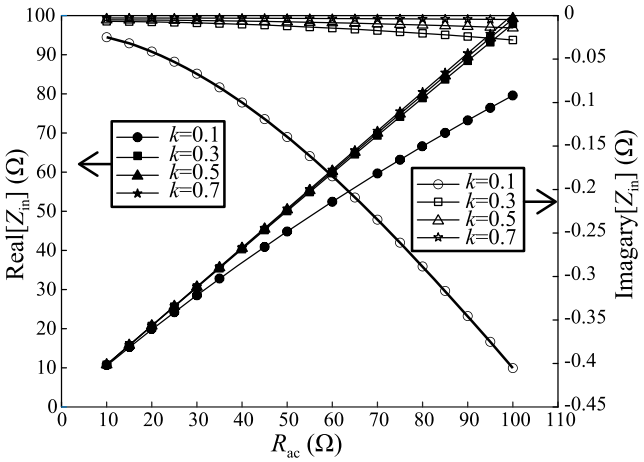

FIGURE 5. Input impedance of a coupled branch shown in Figure 4 under different coupling coefficients.

The ZPA characteristic is realized under such an ideal zero ESR condition. For a nonzero ESR lossy case, the equivalent input impedance of a single branch is derived as follows

$$Z_{in}=\frac{8M^3\omega^3 r+4M^3\omega^3 R_{ac}+2M\omega\left(R_{ac}-2jM\omega\right)r^2}{4M^3\omega^3+\left(2M\omega+jR_{ac}\right)r^2+2M\omega R_{ac}r}. \quad (8)$$

The features of equivalent impedance in a non-ideal case that cannot be simply observed using the closed-form expression; therefore, it requires numerical simulation. Fig. 5 compares the branch input impedance at different coupling coefficients, when r, f, and L are set to 0.407 Ω, 6.78 MHz, and 2.05 μH, respectively. As it can be observed from the figure, with a relatively large coupling coefficient, i.e., when $k \geq 0.3$, the real part of the branch input impedance is almost

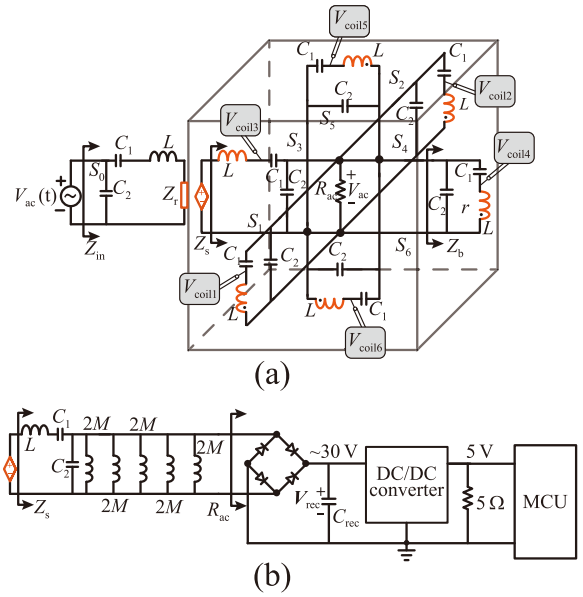

FIGURE 6. Equivalent circuits at a cube connection instant. (a) Default state, in which all branches are connected. (b) The simplified equivalent circuit of one cube considering the digital load.

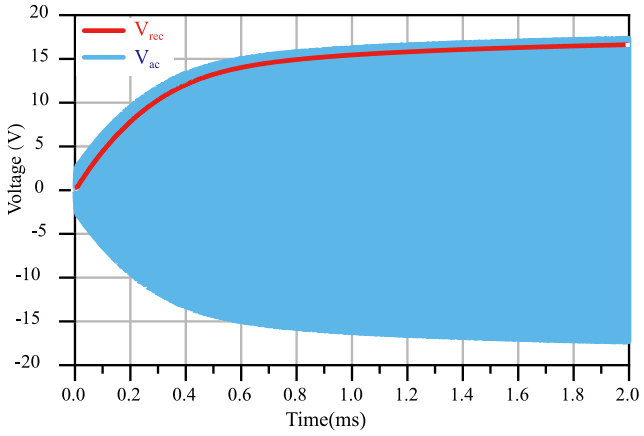

FIGURE 7. Waveform of rectified voltage V_{rec} and ac input voltage V_{ac} in simulation.

linearly proportional to R_{ac}, while the imaginary part is almost negligible. As long as the coupling coefficient between two adjacent coils in this design is about 0.77, larger than 0.3, the branch input impedance is very close to a pure resistive one, i.e., the ZPA characteristic is achieved.

III. CONTROL METHOD

As mentioned in Sub-section II-C, the ZPA characteristic is satisfied only when the uncoupled branches are disconnected. The switches should be turned on or off automatically according to the existence of the corresponding adjacent cubes. An embedded microcontroller (MCU) is utilized to carry out this neighborhood detection. A conventional mobile embedded system is usually powered by batteries [16].

A. TRANSIENT STAGE

In the proposed IPT network, an ac/dc bridge rectifier and the following voltage regulator are utilized in each cube for supplying the digital voltage to the embedded MCU circuit; therefore, no additional battery is needed. Starting from the default state, in which all the switches of the receiver cube's branches are closed, i.e., all branches are connected at the beginning, as shown in Fig. 6(a). If there is no adjacent cube detected, the input impedance of a branch is expressed as follows

$$Z_b = \left(j\omega L + \frac{1}{j\omega C_1}\right) \| \frac{1}{j\omega C_2} = j\omega 2\,M. \tag{9}$$

Therefore, the impedance of an uncoupled branch is inductive. Its inductance is $2M$, as shown in Fig. 6(b). No matter a branch is connected or disconnected, it will not short the load; therefore, such a topology guarantees the safe operation of the circuit. The cube voltage V_{ac} rises when one of the branches is coupled to the existing network. The ac voltage goes across the bridge rectifier and charges the filter capacitor C_{rec}, such that the MCU can be started up when V_{rec} rises above a specific voltage threshold.

In real applications, the equivalent ac load R_{ac} is embodied with a rectifier, a filter capacitor, a dc/dc converter, and a dc load, as illustrated in Fig. 6(b). The ac voltage is rectified to dc voltage through the full bridge rectifier and capacitors. At the relatively light load condition, the rectified dc voltage $V_{rec} = \pi\,|V_{ac}|\,/4$. Fig. 7 shows the transient waveform showing the accumulating charging process of C_{rec}. Within 0.2 milliseconds, the rectified voltage V_{rec} reaches the startup threshold of the dc/dc chip. This embedded MCU is then activated after a constant digital voltage is established and stabilized.

B. DETECTION METHOD

After activation, all cubes keep detecting their branches from time to time to perceive the approaching and detaching events in their neighborhood. If a new inactive cube approaches an activated cube, its secondary-side impedance, as illustrated in Fig. 6(a), can be derived as follows

$$Z_s = \frac{j\omega M}{2} \| R_{ac} + j\omega M = \frac{\omega M\,(3R_{ac} + j\omega M)}{\omega M - 2jR_{ac}}. \tag{10}$$

The reflected impedance looking from the primary-side activated cube is expressed as follows

$$Z_r = \frac{\omega^2 M^2}{Z_s} = \frac{\omega M\,(\omega M - 2jR_{ac})}{3R_{ac} + j\omega M}. \tag{11}$$

The input impedance of the activated cube is obtained as follows

$$Z_{in} = \frac{2\omega M R_{ac}}{4\omega^2 M^2 + 25R_{ac}^2}\,(2\omega M + j5R_{ac}) \tag{12}$$

Eq. (12) demonstrates that when an inactivated cube joins the system, it first introduces an inductive impedance to

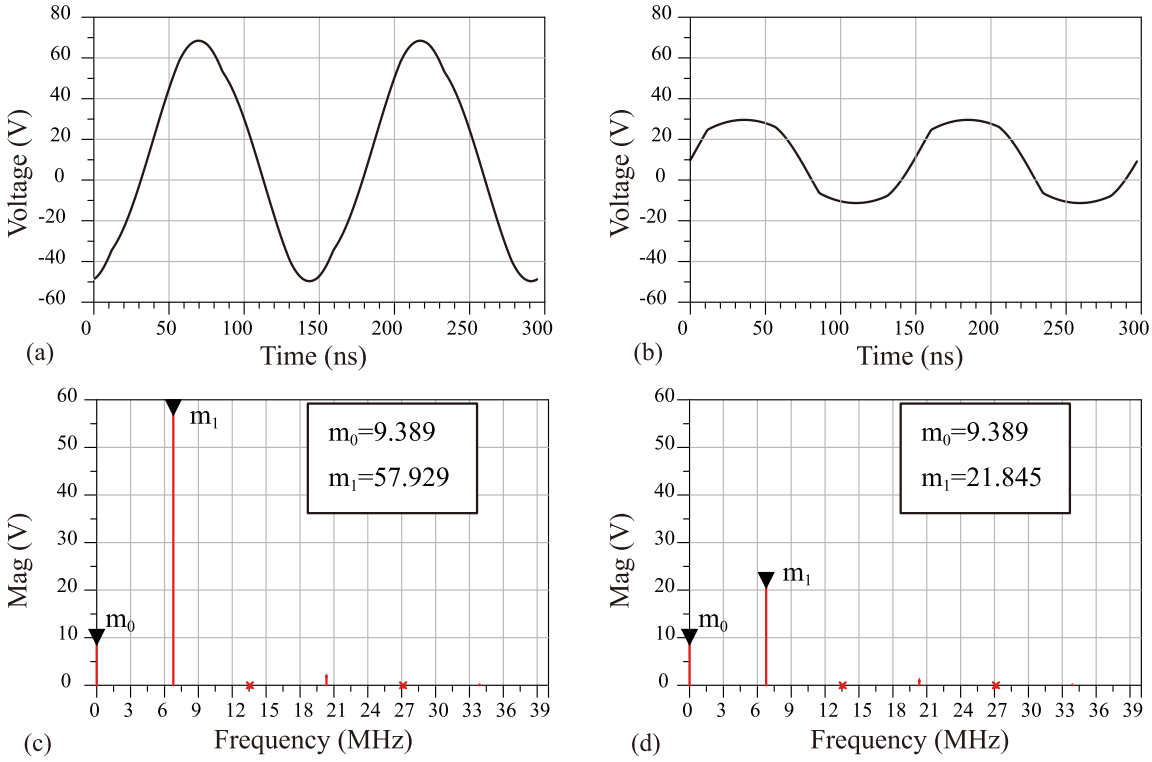

FIGURE 8. Comparison of coil voltages. (a) Voltage waveform with a neighboring cube. (b) Voltage waveform without a neighboring cube. (c) Voltage spectrum with a neighboring cube. (d) Voltage spectrum without a neighboring cube.

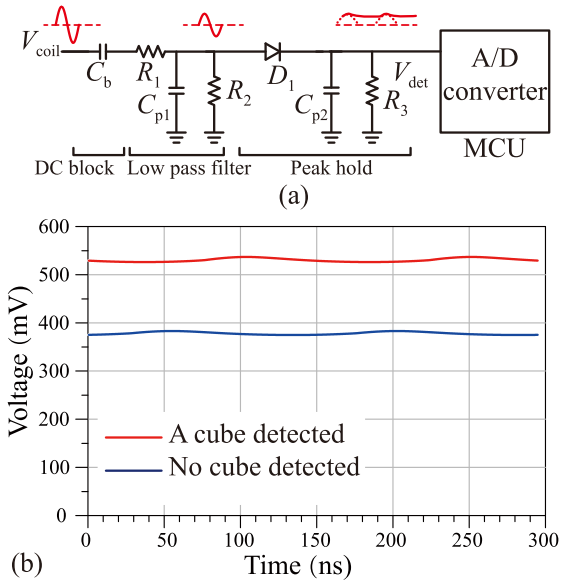

FIGURE 9. Auxiliary circuit and waveform for cube neighborhood detection. (a) AC peak detection circuit. (b) Simulation waveform of V_{det}.

the coupled branch of its relaying neighbor cube. After the embedded MCU is started up, it detects the occupancy of its neighboring slots and disconnects the uncoupled branches, such that its reflected impedance can attain a pure resistive value.

Fig. 8 shows the voltage waveform and spectrum of a branch coil within V_{coil1} to V_{coil6}, whose corresponding probes are shown in Fig. 6(a). When a cube is coupled to one of the branches, the corresponding coil voltage is shown in Fig. 8(a). if no cube approaches, the coil voltage magnitude is much smaller, as shown in Fig. 8(b). From the spectrum shown in Fig. 8(c) and (d), we can see that the dc components with or without a neighboring cube are almost the same. The major difference lies in the magnitudes of their fundamental harmonic. Given this observation, the different information associated with the coil voltage can be used to identify the occupancy of the adjacent face slots of a cube. An ac peak detection circuit is designed for such an identification task. Fig. 9 shows the auxiliary circuit and output waveform. In the circuit, the dc component is firstly filtered by the capacitor C_b. Following that, the high-order harmonics are filtered by a low-pass filter and voltage divider, which are formed by R_1, R_2, and C_{p1}. Finally, the pure ac voltage is converted into dc by a peak detector, which is formed by D_1, C_{p2}, and R_3. The output dc voltage is fed to an analog-to-digital converter (ADC) for quantification and sent to the MCU for generating the corresponding switch control commands.

The cubes first run an initialization program and finalize the configuration according to a specific spatial arrangement. The detection and control processes are summarized as follows. When the MCU is activated, it carries out a neighborhood detection function to identify the coupled or uncoupled branches. The MCU turns off the uncoupled branches.

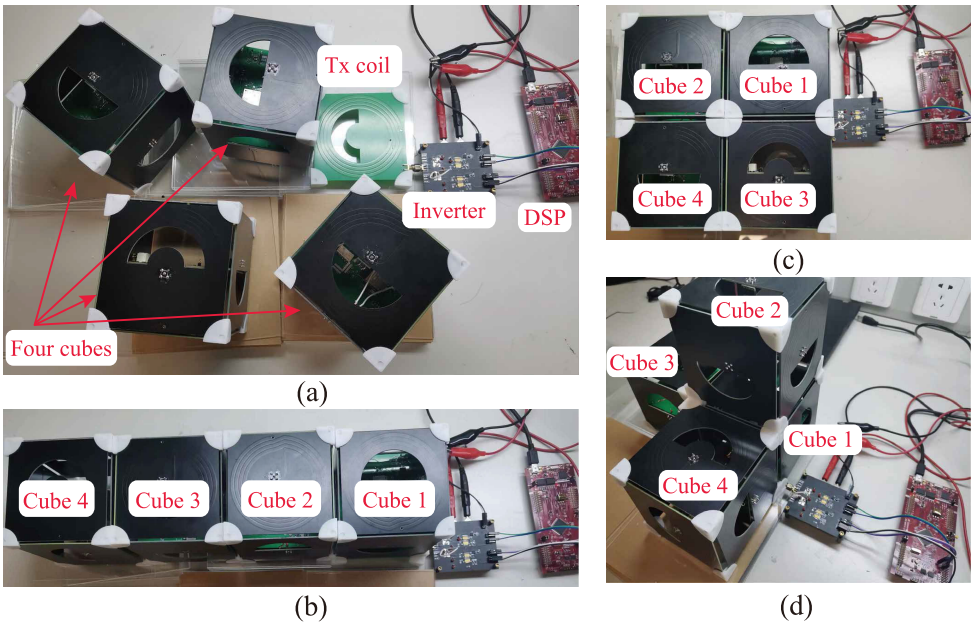

FIGURE 10. Experimental setup and different cubes combination. (a) Experimental setup (before configuration and activation). (b) Combination case I (one-dimensional). (c) Case II (two-dimensional). (d) Case III (three-dimensional).

After an initial delay of three seconds, the reconfigurable process is done.

IV. EXPERIMENT

An experimental fission-type reconfigurable 3D-IPT system with four battery-free cubes is fabricated and tested to evaluate the feasibility and performance of the proposed design. The experimental setup is shown in Fig. 10(a). The prototyped cubes are hollow. All digital components in a conceptual IoT application can be allocated inside the cube. The transmitting coils only occupy the frame surface. The four cubes are configured into one-dimensional [Fig. 10(b)], two-dimensional [Fig. 10(c)], and three-dimensional [Fig. 10(d)] layouts, respectively, for testing the IPT performance in different configurations. The system is powered by a dc power source (WPS3010B, Wanptek Inc.) with a 30 V supply voltage. Each face of a cube has a four-turn PCB coil to form a magnetic coupler with its adjacent cube. A DSP (digital signal processor) evaluation board (LAUNCHXL using TMS320F28377S, Texas Instrument Inc.) is used to generate a high-resolution pulse width modulation (HRPWM) for driving a full bridge inverter. The full bridge inverter is built with four GaN (gallium nitride) switches (GS61008T, GaN System Inc.) and operates at 6.78 MHz. An MCU (ESP32, Espressif Inc.) is programmed to detect and control the active switches in each cube. The MCU inherently includes Bluetooth and Wi-Fi modules, which enables a convenient switch between the reconfigurable state and the stable energy transmission state. The switches are implemented with mechanical relays (TX2SA-L2, Panasonic Inc.). The ratio of the output power to the input power of the selected mechanical relays at isolation and contact conditions at 6.78 MHz are 65 dB and 0.05 dB, respectively, enabling each WPT branch to be completely turned on or off. The high-frequency ac power is rectified to dc power by a rectifier bridge consisting of four discrete diodes (DFLS240L, Diodes Inc.). The output of the diode bridge rectifier is connected to a close-loop regulated buck converter (TPS5430, Texas Instruments Inc.) for providing a 5 V regulated output voltage to the MCU and the extra load. In this study, the extra load in each cube is a 5 Ω resistor. The rated output power of each cube is set to 5 W. The coupling coefficient of any two nonadjacent coils is measured to be less than or equal to 0.068, which is more than ten times smaller than that of two adjacent coils (0.77 in this design). Therefore, the cross-coupling among the nonadjacent coils can be neglected. The parameters of the other passive components are listed in Table 1.

TABLE 1. Parameters of the IPT system.

Parameter	Value	Parameter	Value
V_{DC}	30 V	f	6.78 MHz
L	2.13 μH	C_1	1.24 nF
C_2	167 pF	M	1.65 μH
r	517 mΩ	Q	175.5
k (adjacent)	0.77	Rated power	4 $\times$ 5 W
k (nonadjacent)	$\leq$ 0.068		

TABLE 2. Parameters of the peak-detector circuit.

Parameter	Value/Type	Parameter	Value
C_{b}	10 nF	R_1	10 kΩ
R_2	10 kΩ	R_3	1 kΩ
C_{p1}	10 pF	C_{p2}	47 μF
D_1	NSR0240HT1G		

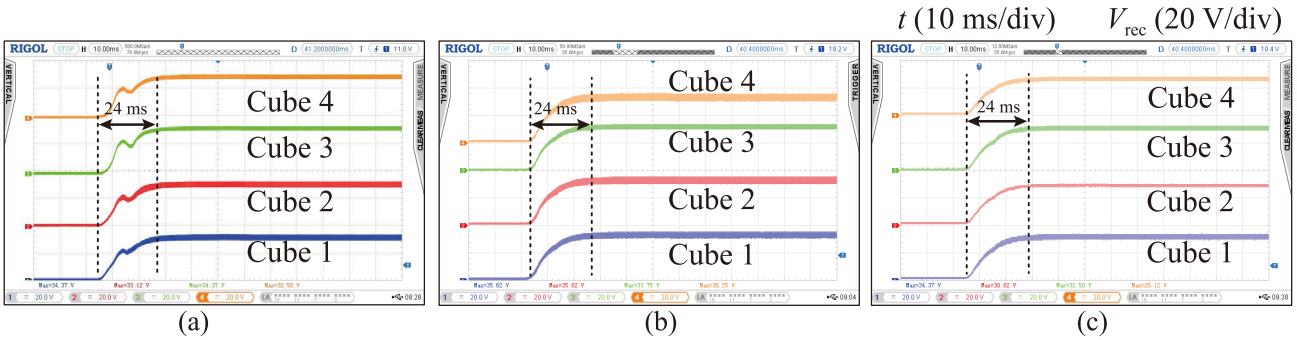

FIGURE 11. Transient processes of rectified voltage V_{rec} after power on. (a) Case I. (b) Case II. (c) Case III.

Moreover, in the transmitter drive, as the full-bridge inverter gives a square-wave voltage output, its compensating capacitor C_2, which is originally placed in parallel with the inverter output and transmitting coil, should be moved to either a cube in the system, such that to avoid the transient short-circuit condition at the switching instants.

A. VALIDATION OF BASIC 3D-IPT FUNCTION

The detection algorithm is implemented by the MCU in each cube. The components' parameters in the ac-peak-detector circuit are listed in Table. 2.

Fig. 11 illustrates the transient processes of the three configurations. The rectified voltage V_{rec} values in the four cubes in the three cases reach their maximum value within 24 ms. It means that the MCUs can properly configure and activate the system within 24 ms. At steady state, the rectified voltages in all cubes and all cases are close to the 30 V input voltage. We can also find that the cubes that are closer to the transmitting coil can more quickly receive sufficient energy and attain a stable state. After a short delay, the coil voltages V_{coil} in each cube reach the steady state, whose voltages are illustrated in Fig. 12(a). The ac component peak of a coil voltage is obtained after being fed into a peak-detector circuit. The output voltage is within the range of ADC input; therefore, it can be quantified by the ADC in the activated MCU. Fig. 12(b) shows the output voltage V_{det} after the peak detection circuit. It is not a constant dc voltage. We use the average value of 60 samples to identify the difference with or without an adjacent cube. If there exists an adjacent cube, the average detection voltage V_{det} of the corresponding branch is about 1.2 V. If there has no adjacent cube, V_{det} is very low, around 150 mV. In this way, the MCUs successfully find out the uncoupled branches and turn off their corresponding switches, such that the transmission efficiency can be optimized.

Fig. 13 shows the steady-state waveform of the ac voltage in each cube. The ac voltage of a cube is out of phase to that of its neighboring coupled cube. In case I, ac voltages in cubes 1 and 3 have the same phase, while those in cubes 2 and 4 are out of phase. In case II, ac voltage in cubes 1 and 4 have the same phase, while those in cubes 2 and 3 are out of phase. In case III, ac voltage in cubes 2, 3, and 4 have the same phase since they are all adjacent to cube 1. The ac voltage magnitudes in all cubes and cases are very close to a constant value.

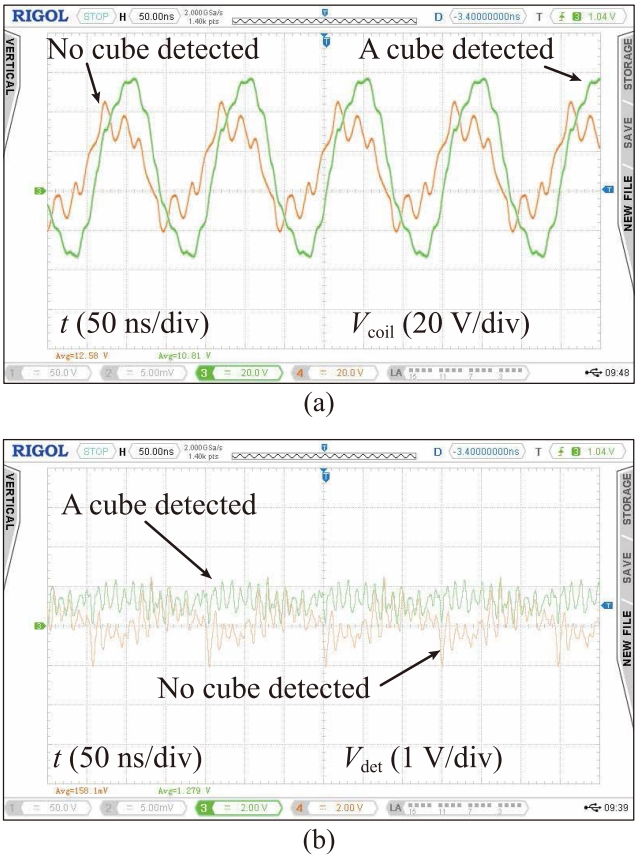

FIGURE 12. Voltage waveform in the neighborhood peak-ac detection circuit. (a) Coil voltage V_{coil}. (b) Detection voltage V_{det}.

B. RELUCTANCE AGAINST LOAD VARIATION

The proposed 3D-IPT circuit topology has an inherent strong rejection to load variation. The output dc voltage is relatively constant under different or fluctuating load resistance. In this experiment, we change R_4 the load resistor of cube 4 from 15 Ω (light load) to 5 Ω (heavy load) in a sudden, while

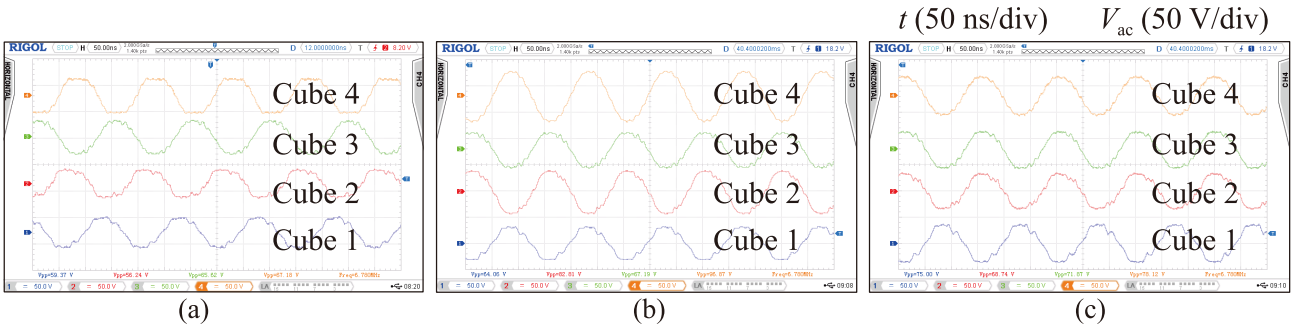

FIGURE 13. AC voltages of different cubes in different cases (a) Case I. (b) Case II (c) Case III.

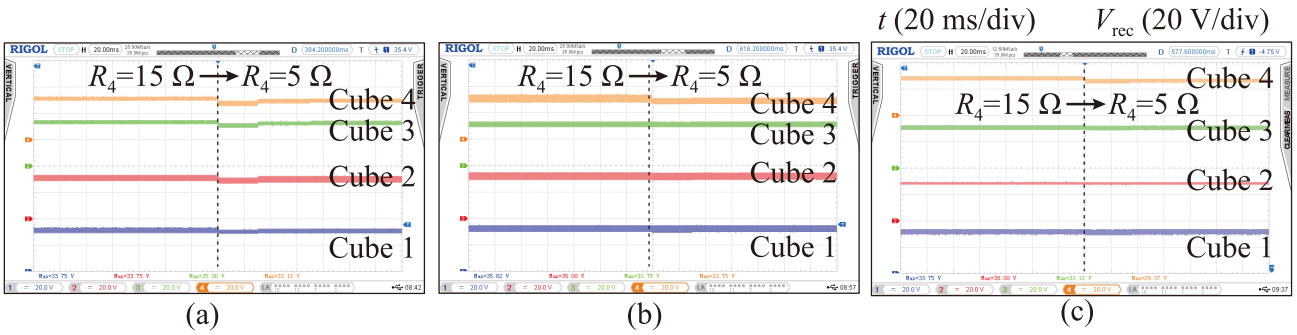

FIGURE 14. Output dc voltages of cube 4 under sudden load variations (a) Case I. (b) Case II (c) Case III.

keeping others load unchanged, i.e., R_1, R_2, and $R_3 = 5\,\Omega$. Fig. 14 shows the rectified dc voltages in the three cases when experiencing sudden load variations. In case I, this load variation causes a slight voltage fluctuation in cube 4, about 4 V out of 30 V, for 30 ms. Such a load variation also influences the rectified voltage in cubes 1, 2, and 3 through the coupling network. The voltage of the cube, which is closer to the transmitting coil, is less affected. After 30 ms, this voltage fluctuation diminishes. In cases II and III, the voltage fluctuation caused by the load change in cube 4 has very little influence on cubes 2 and 3. In general, this system shows a strong load variation rejection ability. Such a unique feature eases the design of the following dc/dc regulator stage.

C. EFFICIENCY AND LOSS ANALYSIS

In this work, the output power is consumed by the external load in each cube. i.e. 5 Ω resistor. Given that the dc/dc regulator supplies a constant 5 V output voltage, the output power is fixed at 5 W in each cube. Therefore, the total output power of the four cubes is 20 W. The power utilization efficiency η is calculated as the ratio of P_{out}, the total dc power of the four extra loads in four cubes after the regulator, to P_{in}, the dc input power before the transmitter inverter

$$\eta = \frac{P_{out}}{P_{in}} = \frac{P_{out}}{P_{loss} + P_{control} + P_{out}} \tag{13}$$

where P_{loss} and $P_{control}$ are the power losses of the power electronics and the microcontroller. The loss power contains conduction and switching losses in the inverter, rectifier, IPT coil links, and dc/dc regulators. The efficiency of IPT coil links is up to 90%–95%. The end-to-end power efficiency of the system under different configurations is listed in Table 3. The efficiency can gain a 2%–3% improvement after detecting the neighborhood availability and optimizing the network by opening the uncoupled branches.

TABLE 3. Power efficiency before and after neighborhood detection and branch optimization.

	Before	After
Case I	60.7%	63.1%
Case II	65.3%	67.9%
Case III	67.2%	70.2%

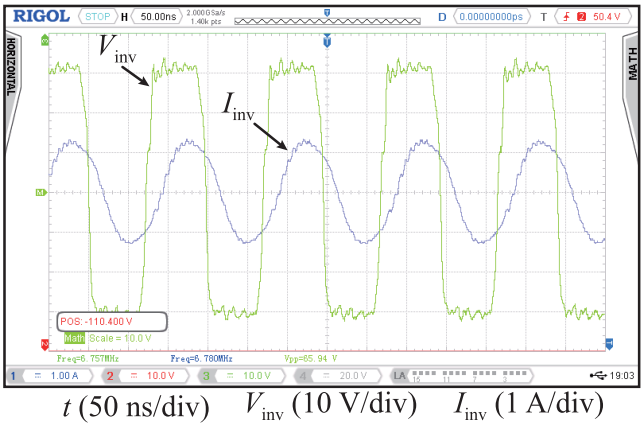

FIGURE 15. Inverter voltage and current waveform.

TABLE 4. Comparison of some typical 3D multi-load WPT systems.

Ref.	Power	Frequency	System efficiency	Coil-link efficiency	Coupling coefficient	CV characteristic	Reconfigurablility
[10]	3–15 W	6.78 MHz	60%–70%	85–95%	0.01–0.1	Yes	-
[12]	3 W	530 kHz	-	50–60%	-	-	-
[13]	1 W	550 kHz	-	69.5%	-	-	-
[16]	5-15 W	6.78 MHz	35%–50%	-	-	-	Yes
This work	20 W	6.78 MHz	60%–70%	90–95%	0.77	Yes	Yes

The voltage and current waveform of the inverter output are illustrated in Fig. 15. The current I_{inv} lags behind the voltage V_{inv} a little bit. Therefore, the zero-voltage switching (ZVS) characteristic can be achieved; the MOSFET switching loss is minimized.

In general, the experimental results prove the feasibility of the proposed system. From the comparison with other state-of-the-art 3D multi-load WPT systems, which is listed in Table 4, the performance of the proposed system is commensurate with other cutting-edge designs. Moreover, this fission-type wireless 3D-IPT design processes a configurable feature, which is promising to support the easy configuration of IoT applications in the future smart home or smart city scenarios.

V. CONCLUSION

In this paper, a fission-type 3D-IPT (three-dimensional inductive power transfer) system was proposed to meet the multiple-device power supply requirements in future ubiquitous and re-configurable IoT applications. A series-parallel (SP) compensation network was utilized to realize the zero phase angle (ZPA) and constant voltage (CV) characteristics in each wireless coupled cube unit. The cubes not only receive power from their upstream cubes but also serve as power relays to wirelessly transfer power to their downstream cubes. The CV property implies a strong load-variation rejection in all cubes. It eases the design of the following voltage regulation stage and the digital load. A neighborhood detection circuit detects the coupling condition of all branches in a cube and turns off those uncoupled branches. Such actions realize the zero-phase-angle (ZPA) property and further improve power utilization efficiency. To validate the proposed idea, a 20 W 3D-IPT experimental system was prototyped and carefully evaluated. The prototype consists of one transmitter and four independent cubes as relays or end-users in any spatial arrangement. The experimental results showed that the coil-link efficiency is above 90%, while the end-to-end transmission efficiency of the whole system ranges from 60% to 70%. The proposed 3D-IPT system provided a new idea and engineering practice for effectively building the 3D reconfigurable IoT array, which is useful for future ubiquitous IoT applications. A very close neighboring position is required between two cubes in this design, such that the compensation condition can be ensured. This restriction of neighboring distance might be loosened in future new designs.

REFERENCES

[1] O. Knecht and J. W. Kolar, "Performance evaluation of series-compensated IPT systems for transcutaneous energy transfer," *IEEE Trans. Power Electron.*, vol. 34, no. 1, pp. 438–451, Jan. 2019.

[2] T. Sasatani, A. P. Sample, and Y. Kawahara, "Room-scale magnetoquasistatic wireless power transfer using a cavity-based multimode resonator," *Nature Electron.*, vol. 4, no. 9, pp. 689–697, Aug. 2021.

[3] S. Jeong, "Smartwatch strap wireless power transfer system with flexible PCB coil and shielding material," *IEEE Trans. Ind. Electron.*, vol. 66, no. 5, pp. 4054–4064, May 2019.

[4] Y. Alwesabi, Z. Liu, S. Kwon, and Y. Wang, "A novel integration of scheduling and dynamic wireless charging planning models of battery electric buses," *Energy*, vol. 230, Sep. 2021, Art. no. 120806.

[5] S. Hasanzadeh and S. Vaez-Zadeh, "Efficiency analysis of contactless electrical power transmission systems," *Energy Convers. Manag.*, vol. 65, pp. 487–496, Jan. 2013.

[6] A. Alliance, "Airfuel resonant wireless power transfer (WPT) system baseline system specification (BSS)," AirFuel Alliance, Tech. Rep. TS-0010-A v2.00, 2017.

[7] J. Wang and W.-H. Liao, "Attaining the high-energy orbit of nonlinear energy harvesters by load perturbation," *Energy Convers. Manag.*, vol. 192, pp. 30–36, Jul. 2019.

[8] K. Yazawa, Y. Feng, and N. Lu, "Conformal heat energy harvester on Steam4 pipelines for powering IoT sensors," *Energy Convers. Manag.*, vol. 244, Sep. 2021, Art. no. 114487.

[9] P. Meyer, P. Germano, M. Markovic, and Y. Perriard, "Design of a contactless energy-transfer system for desktop peripherals," *IEEE Trans. Ind. Appl.*, vol. 47, no. 4, pp. 1643–1651, Jul./Aug. 2011.

[10] J. Feng, Q. Li, and F. C. Lee, "Load detection and power flow control algorithm for an omnidirectional wireless power transfer system," *IEEE Trans. Ind. Electron.*, vol. 69, no. 2, pp. 1422–1431, Feb. 2022.

[11] J. Wu, X. Dai, Y. Sun, and Y. Li, "A node role dynamic change method among repeater, receiver, and decoupling using topology switching in multinode WPT system," *IEEE Trans. Power Electron.*, vol. 36, no. 10, pp. 11174–11182, Oct. 2021.

[12] W. M. Ng, C. Zhang, D. Lin, and S. Y. Ron Hui, "Two- and three-dimensional omnidirectional wireless power transfer," *IEEE Trans. Power Electron.*, vol. 29, no. 9, pp. 4470–4474, Sep. 2014.

[13] C. Zhang, D. Lin, and S. Y. Hui, "Basic control principles of omnidirectional wireless power transfer," *IEEE Trans. Power Electron.*, vol. 31, no. 7, pp. 5215–5227, Jul. 2016.

[14] Y. Gu, J. Wang, Z. Liang, Y. Wu, C. Cecati, and Z. Zhang, "Single-transmitter multiple-pickup wireless power transfer: Advantages, challenges, and corresponding technical solutions," *IEEE Ind. Electron. Mag.*, vol. 14, no. 4, pp. 123–135, Dec. 2020.

[15] D. Ahn and S. Hong, "Effect of coupling between multiple transmitters or multiple receivers on wireless power transfer," *IEEE Trans. Ind. Electron.*, vol. 60, no. 7, pp. 2602–2613, Jul. 2012.

[16] K. Sumiya, T. Sasatani, Y. Nishizawa, K. Tsushio, Y. Narusue, and Y. Kawahara, "Alvus: A reconfigurable 2-D wireless charging system," *Proc. ACM Interact., Mobile, Wearable Ubiquitous Technol.*, vol. 3, no. 2, pp. 1–29, Jun. 2019.

[17] M. Fu, H. Yin, M. Liu, Y. Wang, and C. Ma, "A 6.78 MHz multiple-receiver wireless power transfer system with constant output voltage and optimum efficiency," *IEEE Trans. Power Electron.*, vol. 33, no. 6, pp. 5330–5340, Jun. 2018.

[18] Y. Li, J. Hu, X. Li, and K.-W.-E. Cheng, "A flexible load-independent multi-output wireless power transfer system based on cascaded double T-resonant circuits: Analysis, design and experimental verification," *IEEE Trans. Circuits Syst. I, Reg. Papers*, vol. 66, no. 7, pp. 2803–2812, Jul. 2019.

[19] L. Sun, H. Tang, and S. Zhong, "Load-independent output voltage analysis of multiple-receiver wireless power transfer system," *IEEE Antennas Wireless Propag. Lett.*, vol. 15, pp. 1238–1241, 2015.

[20] C. Cheng, F. Lu, Z. Zhou, W. Li, C. Zhu, H. Zhang, Z. Deng, X. Chen, and C. C. Mi, "Load-independent wireless power transfer system for multiple loads over a long distance," *IEEE Trans. Power Electron.*, vol. 34, no. 9, pp. 9279–9288, Sep. 2019.
[21] Y. Wang, Z. Dongye, H. Zhang, C. Zhu, and F. Lu, "A domino-type load-independent inductive power transfer system with hybrid constant-current and constant-voltage outputs," *IEEE Trans. Power Electron.*, vol. 36, no. 8, pp. 8824–8834, Aug. 2021.
[22] C. Cheng, W. Li, Z. Zhou, Z. Deng, and C. Mi, "A load-independent wireless power transfer system with multiple constant voltage outputs," *IEEE Trans. Power Electron.*, vol. 35, no. 4, pp. 3328–3331, Apr. 2020.
[23] C. Cheng, Z. Zhou, W. Li, J. Lu, Z. Deng, and C. C. Mi, "Long-distance wireless power transfer system powering multiple loads with constant voltage outputs using S-SP compensation," *IET Power Electron.*, vol. 13, no. 9, pp. 1729–1734, Jul. 2020.
[24] C. Cheng, C. Wang, Z. Zhou, W. Li, Z. Deng, and C. C. Mi, "Repeater coil-based wireless power transfer system powering multiple gate drivers of series-connected IGBTs," *IET Power Electron.*, vol. 13, no. 9, pp. 1722–1728, Jul. 2020.
[25] C. Cheng, Z. Zhou, W. Li, Z. Deng, and C. C. Mi, "A power relay system with multiple loads using asymmetrical coil design," *IEEE Trans. Ind. Electron.*, vol. 68, no. 2, pp. 1188–1196, Feb. 2021.

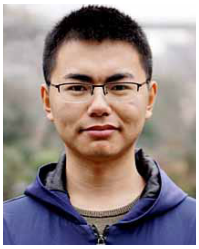

YIMING GAO received the B.S. and B.L. degrees from the Qingdao University of Technology, Qingdao, China, in 2018. He is currently pursuing the Ph.D. degree with ShanghaiTech University, China. His research interests include wireless power transfer, simulation, and design algorithms for power and energy circuits and systems.

ZIJIE CHEN received the B.E. degree in electronic information engineering from Hangzhou Dianzi University, in 2021. He is currently pursuing the master's degree with ShanghaiTech University. His research interests include energy harvesting, battery-free IoT, cyber-electro-mechanical co-design, and TinyML.

HAOYU WANG (Senior Member, IEEE) received the bachelor's degree (Hons.) in electrical engineering from Zhejiang University, Hangzhou, China, in 2009, and the Ph.D. degree in electrical engineering from the University of Maryland at College Park, College Park, MD, USA, in 2014. In 2014, he joined the School of Information Science and Technology, ShanghaiTech University, Shanghai, China, where he is currently a Tenured Associate Professor. His research interests include power electronics, plug-in electric and hybrid electric vehicles, the applications of wide-bandgap semiconductors, renewable energy harvesting, and power management integrated circuits. He is an Associate Editor of IEEE TRANSACTIONS ON INDUSTRIAL ELECTRONICS, IEEE TRANSACTIONS ON TRANSPORTATION ELECTRIFICATION, and *CPSS Transactions on Power Electronics and Applications*.

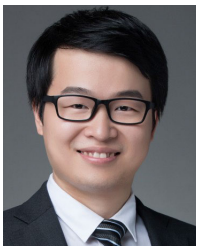

YU LIU (Senior Member, IEEE) received the B.S. and M.S. degrees in electrical engineering from Shanghai Jiao Tong University, Shanghai, China, in 2011 and 2013, respectively, and the M.S. and Ph.D. degrees in electrical engineering from the Georgia Institute of Technology, Atlanta, GA, USA, in 2013 and 2017, respectively.

He is currently a Tenure-Track Assistant Professor with the School of Information Science and Technology, ShanghaiTech University, Shanghai. His current research interests include modeling, protection, fault location, and state/parameter estimation of power systems and power electronic systems.

MINFAN FU (Senior Member, IEEE) received the B.S., M.S., and Ph.D. degrees in electrical and computer engineering from the University of Michigan—Shanghai Jiao Tong University Joint Institute, Shanghai Jiao Tong University, Shanghai, China, in 2010, 2013, and 2016, respectively. From 2016 to 2018, he was a Postdoctoral Researcher with the Center for Power Electronics Systems, Virginia Polytechnic Institute, and State University, Blacksburg, VA, USA. He is currently an Assistant Professor at the School of Information Science and Technology, ShanghaiTech University, Shanghai. He holds one U.S. patent and three Chinese patents, and has authored or coauthored more than 50 papers in prestigious IEEE journals and conferences. His research interests include megahertz wireless power transfer, high-frequency power conversion, high-frequency magnetic design, and the application of wide-bandgap devices. He is currently an Associate Editor of the IEEE IES Industrial Electronics Technology News and serves as the Section Chair for several conferences, such as IECON, IPEMC, and VEH. His conference paper for IECON 2019 won the IES-SYPA Competition. He is the Tutorial Speaker for IPEMC 2020 and ISIE 2020.

JUNRUI LIANG (Senior Member, IEEE) received the B.E. and M.E. degrees in instrumentation engineering from Shanghai Jiao Tong University, Shanghai, China, in 2004 and 2007, respectively, and the Ph.D. degree in mechanical and automation engineering from The Chinese University Hong Kong, Hong Kong, China, in 2010.

He is currently an Associate Professor at the School of Information Science and Technology, ShanghaiTech University, Shanghai. His research interests include energy conversion and power conditioning circuits, kinetic energy harvesting and vibration suppression, the IoT devices, and mechatronics. He was a recipient of three Best Paper Awards in the 2009 and 2010 IEEE International Conference on Information and Automation, and the 2021 International Conference on Vibration Energy Harvesting and Applications, respectively. He is an Associate Editor of *IET Circuits, Devices and Systems* and the General Chair of the 2nd International Conference on Vibration and Energy Harvesting Applications (VEH) 2019.